# A Robust Channel Estimation for Broadband OFDM Systems with Virtual Tones

Weiqing Nie *†, Jianhua Zhang †, Yi Liu †, Feifei Sun †
∗ Wireless Technology Innovation Institute, †Key Laboratory of Universal Wireless Communication, Ministry of Education
Beijing University of Posts and Telecommunications, Beijing 100876, P. R. China
Email: LopezNie@gmail.com

***Abstract*—In broadband orthogonal frequency division multiplexing (OFDM) systems, accurate channel state information (CSI) is required to support coherent detection and diversity combining. However, it is indeed challenging for channel estimation in real systems since some tones are nulled to ease the implementation of spectral masking filters. We propose a novel channel estimation scheme which can solve the leakage caused by virtual tones (VTs) via effective energy compensation and partial refinement with no extra computational complexity. Additionally, the proposed scheme works well with different allocations of various VTs, and hence applicable for hardware realization. Simulation results validate that the proposed method is efficient to combat the leakage, and also robust to the existence of VTs.**

## I. Introduction

The next generation wireless communication systems require a higher data rate to support various multimedia applications. Orthogonal frequency division multiplexing (OFDM) stands as a promising choice to meet this requirement [1] and it has been adopted in the emerging standards, such as IEEE 802.16.m [2] and the 3rd Generation Partnership Project Long Term Evolution Advanced (3GPP LTE-A) [3].

Precise channel state information (CSI) is critical for coherent demodulation. A tremendous amount of work [4], [5] went into channel estimation techniques for broadband OFDM systems. These literature assumed that the systems were fully loaded, i.e., all the tones were modulated. However, in most practical OFDM systems, some tones are turned off to avoid interference with adjacent system and to ease the implementation of spectral masking filter. In the presence of these nulled tones, also referred to as virtual tones (VTs), information of a portion of pilots cannot be acquired, and hence degrades the performance of channel estimation significantly. To combat the negative effects caused by VTs, iteration-based algorithms were proposed in [6], [7]. A pre-set threshold was adopted in [6] to detect significant paths and channel frequency responses (CFRs) were interpolated for VTs. The author of [7] sought to improve the channel estimation accuracy by co-channel interference cancellation with iterations.

Unfortunately, sophisticated processing, e.g., the aforementioned iterative operation, also introduces a higher complexity into channel estimators. In this paper, we propose an enhanced discrete Fourier transform based (DFT-based) channel estimation scheme to achieve a good performance yet with low complexity. From theoretical analysis, one can see clearly that the energy leakage disperses all over the tones and especially for those activated tones (ATs) close to VTs. Aiming to overcome these negative effects caused by VTs, we introduce a novel channel estimation method: energy compensated DFT-based channel estimation with partial refinement (ECDFT-PR). A mirror-symmetric energy compensation is conducted to create artificial CFRs for virtual pilots (VPs), taking advantage of the high correlation of CFRs for tones close to each other. A linear transform for smoothing is then performed in the time-domain to reduce the noise. After the DFT-interpolation, estimation results are transformed back to the frequency-domain. In particular, we refine a part of CFRs for ATs close to VTs appropriately to improve the overall channel estimation performance. Besides, analysis shows that the proposed scheme requires a very low computational complexity and thus suitable for hardware implementation in practical systems.

The rest of the paper is structured as follows: Section II depicts the system model. A theoretical analysis of the DFT-based channel estimation is given in Section III. The proposed algorithm is described and the complexity issue is addressed in Section IV. Simulation results under cases of different quantities and allocations of VTs are reported in Section V. Finally, a conclusion is drawn in Section VI.

## II. OFDM System Model

In this contribution, we consider a broadband OFDM system. The system employs $N$ tones, which consist of $N_{at}$ ATs and $N_{vt}$ VTs ($N = N_{at} + N_{vt}$). ATs are used for data and pilot transmission whereas other tones on the edge of the spectrum are nulled. Furthermore, some tones might also be nulled if their frequencies are known to experience strong interferences.

The channel between the transmitter and the receiver is assumed to be block Rayleigh-fading and remains constant during an OFDM symbol. Therefore, the channel impulse response (CIR) can be written as

$$h(n) = \sum_{l=0}^{L-1} \alpha_l \delta(n - \tau_l), \tag{1}$$

where $L$ denotes the number of paths, the *l-th* path gain $\alpha_l$ is complex Gaussian random variable with zero mean and unit variance. $\tau_l$ represents the corresponding path delay. All the channel taps are assumed to be uncorrelated.

978-1-4244-3574-6/10/$25.00 ©2010 IEEE

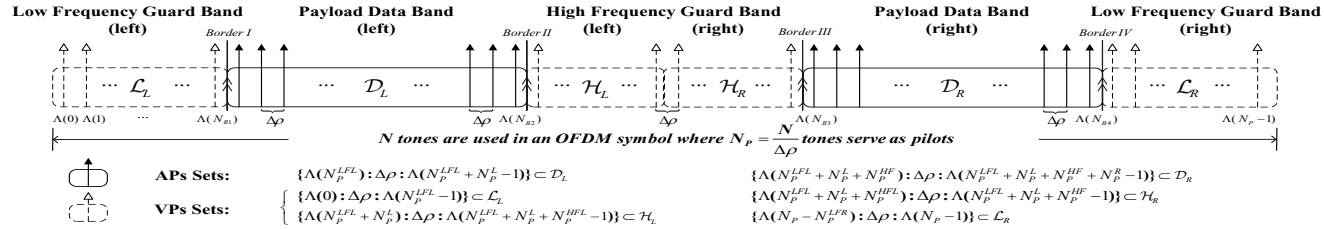


Fig. 1. Pilot allocation with VTs located in both LFGB and HFGB.

At the receiver, with perfect synchronization and OFDM demodulation, the frequency-domain symbol is formulated as

$$Y(k) = X(k)H(k) + W(k),\ k = 0, 1,\ \dots,\ N-1, \tag{2}$$

where $X(k)$, $H(k)$, $W(k)$ denote the transmitted signal, the channel coefficients and the additive white Gaussian noise (AWGN) with zero mean and variance of $\sigma_w^2$, respectively.

In order to support channel estimation, pilot symbols are transmitted along with data. And Fig. 1 illustrates the pilot allocation in an OFDM symbol with VTs existed. As shown, the $N$ tones can be classified into two activated sets ($\mathcal{D}_L$, $\mathcal{D}_R$), as drawn in solid lines, and four virtual sets ($\mathcal{L}_L$, $\mathcal{H}_L$, $\mathcal{H}_R$, $\mathcal{L}_R$), as drawn in dashed lines. And the six tone sets correspond to the left payload data band (PLDB), right PLDB, left low frequency guard band (LFGB), left high frequency guard band (HFGB), right HFGB, and right LFGB, respectively. In real broadband systems, e.g., with a bandwidth of 100 MHz, intermediate frequency (IF) sampling will incur the need to employ expensive high-speed analog to digital converter (ADC). As a result, the baseband sampling is a cost-effective alternative for IF sampling. However, for the baseband sampling, some low frequency tones near the direct current (DC) tone are nulled due to the imperfectness of low-pass filter and coupling in radio frequency (RF) components. Therefore, pilots in $\mathcal{L}_L$, $\mathcal{H}_L$, $\mathcal{H}_R$ and $\mathcal{L}_R$ are reserved as VPs. Assuming that the pilot spacing is $\Delta\rho$ and $\Lambda(\cdot)$ represents the equidistant PTs position in an OFDM symbol. Let $N_P^L$ and $N_P^R$ denote the number of activated pilots (APs) in $\mathcal{D}_L$ and $\mathcal{D}_R$, respectively. $N_P^{LFL}$, $N_P^{HFL}$, $N_P^{HFR}$ and $N_P^{LFR}$ represent the number of VPs in $\mathcal{L}_L$, $\mathcal{H}_L$, $\mathcal{H}_R$ and $\mathcal{L}_R$, separately. Therefore, the total number of PTs $N_P = N_P^{LFL} + N_P^L + N_P^{HFL} + N_P^{HFR} + N_P^R + N_P^{LFR}$. As shown in [8], [9] that equispaced PTs are optimal in terms of the mean square error (MSE) of channel estimation for OFDM systems. However, in the presence of VTs, certain tones consequentially fall into the nulled spectrum and the equidistant prerequisite fails to be met. Those unobtainable CFRs degrade the DFT-based channel estimation performance considerably.

## III. Theoretical Analysis of MSE performance of the DFT-Based Channel Estimation and Energy Leakage

### A. MSE performance of the DFT-Based Channel Estimation

In the presence of VPs, only CFRs on APs can be obtained. Stemming from Eq. (2), the least square (LS) estimation, which is the initial estimation for the DFT-based channel estimation, can be expressed as

$$\hat{H}_{LS}^{vp}(k) = \begin{cases} X_P^H(k)Y_P(k) = H_P(k) + W_{LS}(k) & ,k \in \mathcal{D}_L \cup \mathcal{D}_R, \\ 0 & ,k \in others. \end{cases} \tag{3}$$

where $\mathbf{X}_P$ denotes the $N_P \times N_P$ diagonal matrix containing the transmitted pilots, satisfying $\mathbf{X}_P^H\mathbf{X}_P = \mathbf{I}_{N_P}$. $\mathbf{I}_{N_P}$ represents the identity $N_P \times N_P$ matrix and $\{\cdot\}^H$ stands for the conjugate transpose. $\mathbf{Y}_P$ is the receiving vector on PTs and $\mathbf{H}_P$ stands for the true CFRs vector for PTs. $\mathbf{W}_{LS} = \mathbf{X}_P^H\mathbf{W}$ denotes the LS estimation error.

Eq. (3) can be viewed as band-pass filtering the original LS estimation and thereby can be reformulated in matrix form as

$$\hat{\mathbf{H}}_{LS}^{vp} = \mathbf{H}_P - \mathbf{H}^{vp} + \mathbf{W}_{LS}, \tag{4}$$

where $\mathbf{H}^{vp}$ represents the true CFRs for VPs, i.e., only considering the nonzero values on VPs.

A noise reduction transform $\mathbf{S}$ is performed on the LS estimation in the time-domain, where the channel power concentrates on a relatively small number of taps (significant paths). $\mathbf{S}$ contains only the $L$ significant paths whereas other taps are treated as noise and ignored. After the DFT-interpolation, estimation results are transformed back to the frequency-domain, yielding

$$\begin{aligned} \hat{\mathbf{H}}_{DFT}^{vt} &= \tilde{\mathbf{F}}\mathbf{S}\mathbf{Q}\hat{\mathbf{H}}_{LS}^{vp} = \tilde{\mathbf{F}}\mathbf{S}\mathbf{Q}(\mathbf{H}_P - \mathbf{H}^{vp} + \mathbf{W}_{LS}) \\ &= \mathbf{H} + \tilde{\mathbf{F}}\mathbf{S}\mathbf{Q}(\mathbf{W}_{LS} - \mathbf{H}^{vp}), \end{aligned} \tag{5}$$

where $\tilde{\mathbf{F}}$ is the truncated matrix of the DFT matrix $\mathbf{F}$ and has entries of $\tilde{F}_{m,n} = \exp[\frac{-j2\pi(m-1)(n-1)}{N}]$, $m = 1, 2, ..., N, n = 1, 2, ..., N_P$. $\mathbf{S}$ is a diagonal $N_P \times N_P$ matrix whose diagonal elements corresponding to the $L$ significant paths are set to 1, otherwise 0. The inverse DFT (IDFT) matrix $\mathbf{Q}$ has entries of $Q_{m,n} = \frac{1}{N_P}\exp[\frac{j2\pi(m-1)(n-1)}{N_P}]$, $m, n = 1, 2, ..., N_P$. $\mathbf{H}$ denotes the true CFRs on all the $N$ tones.

In the presence of VTs, the orthogonality of DFT-IDFT processes is lost. Leakage spreads across the channel taps, resulting in severe performance degradation and the channel estimation error $\Delta\mathbf{H}$ is

$$\Delta\mathbf{H} = \tilde{\mathbf{F}}\mathbf{S}\mathbf{Q}(\mathbf{W}_{LS} - \mathbf{H}^{vp}) = \tilde{\mathbf{A}}(\mathbf{W}_{LS} - \mathbf{H}^{vp}) = \tilde{\mathbf{A}}\mathbf{W}_{LS} - \mathbf{I}_{leak}, \tag{6}$$

where $\tilde{\mathbf{A}} = \tilde{\mathbf{F}}\mathbf{S}\mathbf{Q}$ and $\mathbf{I}_{leak}$ stands for the energy leakage over the channel taps. Eq. (6) manifests the estimation error consisting of noise and leakage. The auto-covariance matrix of the estimation error and the average MSE are given as

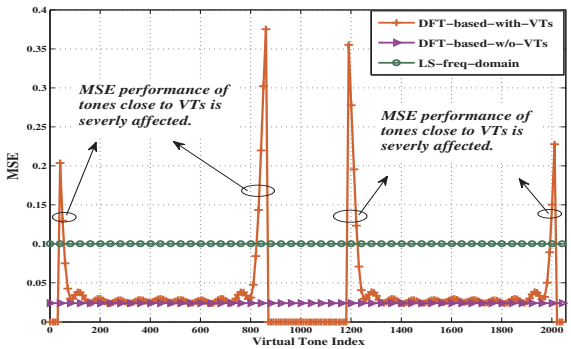


Fig. 2. Numerical results of MSE at SNR=10dB. Total tones number $N = 2048$, which consists of 1664 ATs and 384 VTs. 320 VTs are located in HFGB whereas 64 VTs are in LFGB. The channel response length $L = 24$.

$$\begin{aligned} \mathbf{R}^{with\ vt}_{\Delta H \Delta H} &= E\{\Delta\mathbf{H}\Delta\mathbf{H}^H\} \\ &= \sigma_w^2 \tilde{\mathbf{A}}\tilde{\mathbf{A}}^H + \tilde{\mathbf{A}}\mathbf{R}_{H^{vp}H^{vp}}\tilde{\mathbf{A}}^H, \qquad (7) \\ MSE &= \frac{1}{N} tr\{\mathbf{R}^{with\ vt}_{\Delta H \Delta H}\} \\ &= \frac{L}{N}\sigma_w^2 + \frac{1}{N} tr\{\tilde{\mathbf{A}}\mathbf{R}_{H^{vp}H^{vp}}\tilde{\mathbf{A}}^H\}, \qquad (8) \end{aligned}$$

where $\mathbf{R}_{H^{vp}H^{vp}}$ represents the auto-covariance matrix of CFRs on VPs. The normalized entries of the auto-covariance matrix of $\mathbf{H}_P$ (CFRs on PTs) can be derived as

$$E\{H_P(m)H_P{}^*(n)\} = \begin{cases} 1 & , m = n, \\ \frac{1}{L}\frac{\sin[\frac{\pi(n-m)L}{N_P}]}{\sin[\frac{\pi(n-m)}{N_P}]}\exp[\frac{j\pi(n-m)(L-1)}{N_P}] & , m \neq n. \end{cases} \qquad (9)$$

Utilizing the results from Eq. (9), entries of $\mathbf{R}_{H^{vp}H^{vp}}$ in Eq. (8) can be calculated and the MSE performance can be evaluated.

Fig. 2 shows the numerical results of the MSE analyzed above. It is seen that the MSE performance of ATs close to VTs is severely affected. In particular, the performance of these edge tones can be even worse than that of the LS estimator.

### B. Energy Leakage Analysis

Based on the analysis above, the DFT-based channel estimator performance degrades significantly owing to the energy leakage. Here, we further investigate the leakage shown in Eq. (6). The energy leakage on the *k-th* tone can be derived as

$$\begin{aligned} I_{leak}(k) &= \tilde{\mathbf{A}}_k \mathbf{H}^{vp} \\ &= \frac{1}{N_P}\sum_{n=0}^{L-1} \mathrm{e}^{-j\frac{2\pi}{N}nk} \sum_{m=0}^{N_P-1} H^{vc}(m)\mathrm{e}^{j\frac{2\pi}{N_P}mn}, \qquad (10) \end{aligned}$$

where $\tilde{\mathbf{A}}_k$ represents the *k-th* row of $\tilde{\mathbf{A}}$. Since VPs are located in $\mathcal{L}_L$, $\mathcal{H}_L$, $\mathcal{H}_R$ and $\mathcal{L}_R$, the leakage can be split into four items

$$\begin{aligned} I_{leak1}(k) &= \frac{1}{N_P}\sum_{l_1=1}^{N_P^{LFL}} H(\Lambda(N_{B1}-l_1))\Theta_1(k,l_1)\mathrm{e}^{j\pi(L-1)(\frac{N_{B1}-l_1}{N_P}-\frac{k}{N})}, \\ I_{leak2}(k) &= \frac{1}{N_P}\sum_{l_2=1}^{N_P^{HFL}} H(\Lambda(N_{B2}+l_2))\Theta_2(k,l_2)\mathrm{e}^{j\pi(L-1)(\frac{N_{B2}+l_2}{N_P}-\frac{k}{N})}, \\ I_{leak3}(k) &= \frac{1}{N_P}\sum_{l_3=1}^{N_P^{HFR}} H(\Lambda(N_{B3}-l_3))\Theta_3(k,l_3)\mathrm{e}^{j\pi(L-1)(\frac{N_{B3}-l_3}{N_P}-\frac{k}{N})}, \\ I_{leak4}(k) &= \frac{1}{N_P}\sum_{l_4=1}^{N_P^{LFR}} H(\Lambda(N_{B4}+l_4))\Theta_4(k,l_4)\mathrm{e}^{j\pi(L-1)(\frac{N_{B4}+l_4}{N_P}-\frac{k}{N})}, \end{aligned} \qquad (11)$$

and uniformly we denote

$$\Theta_i(k,l_i) = \frac{\sin[\pi L(\frac{N_{Bi}+(-1)^i l_i}{N_P} - \frac{k}{N})]}{\sin[\pi(\frac{N_{Bi}+(-1)^i l_i}{N_P} - \frac{k}{N})]} \quad , \ i = 1,2,3,4, \qquad (12)$$

where $N_{B1} = N_P^{LFL}$, $N_{B2} = N_P^{LFL} + N_P^L - 1$, $N_{B3} = N_P^{LFL} + N_P^L + N_P^{HFL} + N_P^{HFR}$, $N_{B4} = N_P - N_P^{LFR} - 1$. $\Lambda(N_{B1})$, $\Lambda(N_{B2})$, $\Lambda(N_{B3})$ and $\Lambda(N_{B4})$ indicate the positions of borders between $\mathcal{L}_L$ and $\mathcal{D}_L$, $\mathcal{D}_L$ and $\mathcal{H}_L$, $\mathcal{H}_R$ and $\mathcal{D}_R$, $\mathcal{D}_R$ and $\mathcal{L}_R$, respectively.

Clearly, $(\frac{N_{Bi}+(-1)^i l_i}{N_P} - \frac{k}{N}) \to 0$ as $k$ approaches both side-borders of $\mathcal{D}_L$ and $\mathcal{D}_R$. Therefore, we have the approximation when $k$ comes close to the edge of PLDB:

$$\Theta_i(k,l_i) \approx L\sin c[L(\frac{N_{Bi}+(-1)^i l_i}{N_P} - \frac{k}{N})] \quad , i = 1,2,3,4. \qquad (13)$$

It is obvious that $\Theta_i(k,l_i)$ (i = 1,2,3,4) increase dramatically as $k$ approaching the corresponding side-border of $\mathcal{D}_L$ and $\mathcal{D}_R$. Consequently, the four sub-leakage items $I_{leaki}(k)$ (i = 1,2,3,4) increase considerably. In summary, the energy leakage issue can be very severe, especially for ATs on the edge of PLDB. The phenomenon is hereby known as the "edge effect".

## IV. Energy Compensated DFT-Based Channel Estimation With Partial Refinement

### A. Proposed Channel Estimation Method

Bearing the "edge effect" in mind, we propose an enhanced DFT-based channel estimation—ECDFT-PR. The basic idea behind our proposed method is to compensate the energy leakage via creating artificial CFRs for VPs. In particular, the energy compensation is conducted mirror-symmetrically, which mitigates the discontinuities of CFRs at borders of PLDB more effectively. Moreover, as Eq. (8)–(9) show, the MSE performance for the ATs on the edge of PLDB is severely affected. Therefore, a partial refinement for these edge tones is performed to improve the overall MSE performance. Our proposed method can be described in detail as follows:

*1) The first step:* LS estimation for initial results

The LS estimation is first carried out based on Eq. (3)

$$\hat{\mathbf{H}}^{vp}_{LS} = [\hat{\mathbf{H}}^L_{LS}; \hat{\mathbf{H}}^R_{LS}], \qquad (14)$$

where $[\mathbf{A};\mathbf{B}]$ denotes the vertical concatenation of two matrices $\mathbf{A}$ and $\mathbf{B}$. $\hat{\mathbf{H}}^L_{LS}$, $\hat{\mathbf{H}}^R_{LS}$ represent the LS estimations on the left and the right side of PLDB, respectively.

*2) The second step:* Energy compensation for leakage

Our approach seeks to alleviate the leakage effect with energy compensation for VPs—generating artificial CFRs. Artificial CFRs are created from the LS results of APs near VPs, taking advantage of the high correlation of CFRs for tones close to each other. We have the full $N_P$ points LS estimation as

$$\hat{H}^{full}_{LS}(k) = \begin{cases} \hat{H}^L_{LS}(N_P^{LFL} - k) & , k \in \mathcal{K}_1, \\ \hat{H}^L_{LS}(k - N_P^{LFL}) & , k \in \mathcal{K}_2, \\ \hat{H}^L_{LS}(N_P^{LFL} + 2N_P^L - k - 2) & , k \in \mathcal{K}_3, \\ \hat{H}^R_{LS}(N_P - N_P^{LFR} - N_P^R - k) & , k \in \mathcal{K}_4, \\ \hat{H}^R_{LS}(k - N_P + N_P^{LFR} + N_P^R) & , k \in \mathcal{K}_5, \\ \hat{H}^R_{LS}(N_P - N_P^{LFR} + N_P^R - k - 2) & , k \in \mathcal{K}_6, \end{cases} \qquad (15)$$

where the subsets are defined as: $\mathcal{K}_1 = \{k|0 \le k < N_{B1}\}$; $\mathcal{K}_2 = \{k|N_{B1} \le k < N_{B2}+1\}$; $\mathcal{K}_3 = \{k|N_{B2}+1 \le k < N_{B2}+N_P^{HFL}+1\}$; $\mathcal{K}_4 = \{k|N_{B3}-N_P^{HFR} \le k < N_{B3}\}$; $\mathcal{K}_5 = \{k|N_{B3} \le k < N_{B4}+1\}$; $\mathcal{K}_6 = \{k|N_{B4}+1 \le k < N_P\}$.

It is much easier to view $\hat{\mathbf{H}}_{LS}^{full}$ in this way: subsets of CFRs close to VPs are selected and artificial CFRs are mirror-symmetric with the selected ones. For instance, the selected subset of CFRs is flipped along the axis of $k = N_P^{LFL}$ to generate artificial CFRs for VPs located in $\mathcal{L}_L$. Similarly, artificial CFRs for $\mathcal{L}_R$, $\mathcal{H}_L$ and $\mathcal{H}_R$ can be created by the means shown in Eq. (15).

*3) The third step:* Noise reduction in the time-domain

Exploiting the property of the concentration of channel power, the noise can be reduced efficiently in the time-domain. With proper cyclic prefix (CP) design, we can detect the significant paths without the knowledge of path delay, i.e., keeping only CP length of CIRs. The noise reduction transform $\mathbf{S}$ can be seen as a simple low-pass filter, which eliminates the noise outside the pass-band and in turn means the elimination of most of the noise on the estimated tones. The DFT-interpolation is then applied to the remaining CIRs:

$$\hat{\mathbf{H}}_{DFT}^{vt} = \tilde{\mathbf{F}}\mathbf{S}\mathbf{Q}\hat{\mathbf{H}}_{LS}^{full}. \tag{16}$$

*4) The fourth step:* Partial refinement in the frequency-domain

More insight into Eq. (8)–(9) reveals that the MSE performance for ATs close to VTs is severely affected, even worse than the LS estimation's performance. A partial refinement for these ATs can improve the overall MSE performance effectively. To this end, we substitute an amount of CFRs with the pre-estimated LS results. The number of ATs performed substitution can be calculated as

$$\begin{aligned} S_L &= \arg\max_{S_L}\{\frac{\sum_{ii=1}^{S_L}\Delta H(\frac{N_{at}}{2}\pm ii)\Delta H^*(\frac{N_{at}}{2}\pm ii)}{S_L} > MSE^{LS}\}, \\ S_R &= \arg\max_{S_R}\{\frac{\sum_{jj=1}^{S_R}\Delta H((N_{at}\pm jj))_{N_{at}}\Delta H^*((N_{at}\pm jj))_{N_{at}}}{S_R} > MSE^{LS}\}, \end{aligned} \tag{17}$$

where $S_L$ and $S_R$ represent the number of substituted ATs on each side of PLDB, respectively. $((U))_N$ denotes the modular arithmetic by $N$ and $MSE^{LS}$ is derived in [10]. In conclusion, the final CFRs consist of two parts—the refined CFRs for the edge ATs and CFRs obtained by $\hat{\mathbf{H}}_{DFT}^{vt}$ for the rest of ATs.

## B. Complexity Analysis

For the complexity analysis, we evaluate the ECDFT-PR estimator along with two conventional DFT-based estimators (Estimator $A$, $B$) [10] in terms of the complex multiplications (CMs) involved. Assuming the DFT/IDFT is implemented with the Radix-4 fast Fourier transform (FFT) algorithm which needs $\frac{3}{8}N\log_2 N$ CMs for the $N$ points FFT. The number of CMs and stored coefficients required by the three aforementioned channel estimators are summarized in Table I. A particular case of $N_P = 512$ pilots and CP length $L_{CP} = 256$ (with $N_P$ pilots which consist of $N_P^L = N_P^R = 208$ APs and $N_P^{LF} = 16, N_P^{HF} = 80$ VPs) is also listed in Table I. From Table I, one can see that the complexity of the proposed estimator is much lower than that of Estimator $A$ and $B$. Only few memory units are required to store the pre-estimated coefficients which are used to create the artificial CFRs and to refine the estimations for the edge tones. And as analyzed before, one can see that the proposed estimator gives the best performance in the presence of VTs. Additionally, the proposed estimator needs no perfect knowledge of channel statistics which is demanded by Estimator $A$ and $B$ [10]. Therefore, the proposed method is especially suitable for hardware realization.

TABLE I
*Complexity Comparison of Different Channel estimators*

| | General Case | | Particular Case | |
|---|---|---|---|---|
| Esti. | CMs | Coef. | CMs | Coef. |
| $A$ | $N_P^L+N_P^R+3/8N_P\log_2 N_P$ $+L_{CP}^2+3/8N\log_2 N$ | *N.A.* | 76128 | *N.A.* |
| $B$ | $N_P^L+N_P^R+3/8N_P\log_2 N_P$ $+L_{CP}+3/8N\log_2 N$ | *N.A.* | 10848 | *N.A.* |
| *ECDFT-PR* | $N_P^L+N_P^R+3/8N_P\log_2 N_P$ $+3/8N\log_2 N$ | $N_P^{LF}+N_P^{HF}+$ $2\times(R_L+R_H)$ | 10592 | 176 |

TABLE II
*Main System Parameters*

| | | | |
|---|---|---|---|
| Center Frequency | 5.25GHz | Num. of Total Tones ($N$) | 2048 |
| Channel Bandwidth | 100MHz | Num. of ATs ($N_{at}$) | 1664 |
| Sampling Rate | 122.88MHz | Num. of VTs ($N_{vt}$) | 384 |
| Modulation Scheme | 16QAM | CP Length | 256 |
| Radio Channel | UMa | Pilot Spacing | 4 |

## V. Simulation Results

In this section, the performance of the proposed channel estimation is verified by simulations and the main parameters of the system are listed in Table II. The radio channel is modeled as Urban Macrocell (UMa) scenario recommended by ITU-R [11] with a bandwidth of 100 MHz.

In Fig. 3, the MSE performance of the proposed channel estimation is compared with that of other schemes. Note that the DFT-based estimator with zero-padding suffers an obvious MSE error floor and this phenomenon can be

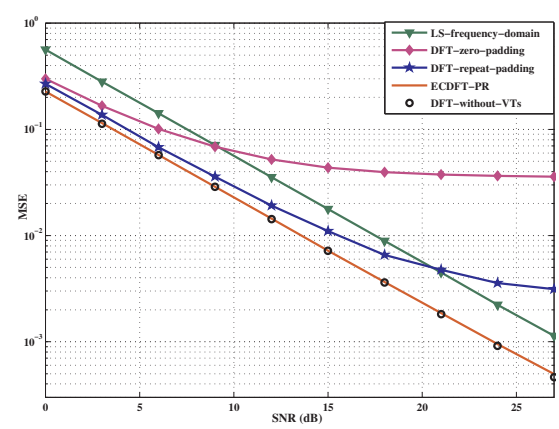


Fig. 3. MSE comparison of different channel estimation schemes.

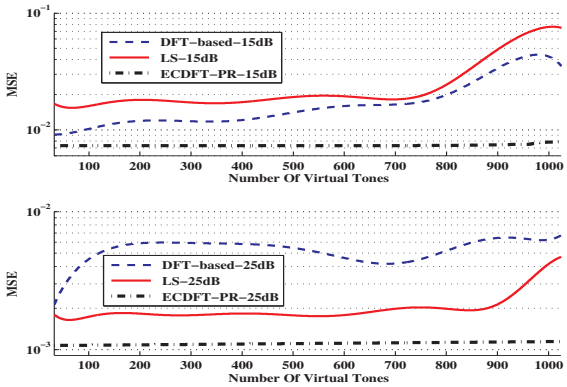


Fig. 4. MSE comparison versus different quantities of VTs.

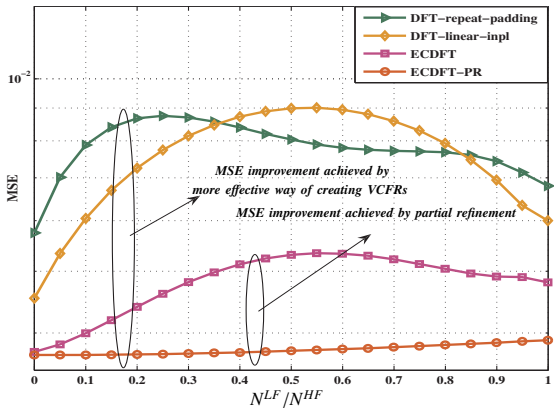


Fig. 5. MSE comparison versus different allocations of VTs.

attributed to the energy leakage caused by VTs. The leakage is mitigated to a certain extent for the DFT-based estimator via generating artificial CFRs with repeat-padding. Evidently, our proposed channel estimator gives the best performance, achieving MSE=$10^{-3}$ at SNR=24dB. For comparison, the performance curve of the DFT-based estimator without VTs is also plotted. As can be seen, the performance degradation of the proposed estimator is negligible.

In order to assess the estimator's robustness to various VTs, the MSE performance under fixed SNRs is shown in Fig. 4. Two cases of fixed SNRs at 15dB and 25dB are provided for the comparison between the medium and the high SNRs. As Fig. 4 illustrates, in both cases, the proposed scheme reveals a better robustness, tracking the increase of VTs almost steadily. In contrast, the MSE curves for the LS estimator and the DFT-based estimator fluctuate intensely as the number of VTs increases, failing to adapt to the variation of VTs.

Fig. 5 illustrates the robustness of the proposed method to different allocations of VTs. The number of VTs located in LFGB indicates different hardware capabilities for different systems. Generally, the number of VTs in LFGB ($N^{LF}$) will not exceed that in HFGB ($N^{HF}$). In Fig. 5, the MSE performances of the proposed method and three other schemes are presented versus the ratio $N^{LF}/N^{HF}$. The proposed ECDFT-PR and ECDFT schemes outperform the other two schemes, which demonstrates the effectiveness of the energy compensation. Moreover, the performance is enhanced by the partial refinement, especially when $N^{LF}/N^{HF}$ increases. From Fig. 5, the proposed channel estimation is shown insensitive to different allocations of VTs.

## VI. Conclusions

In this paper, a novel channel estimation for broadband OFDM systems with VTs is presented. Effective energy compensation and partial refinement are introduced to eliminate the energy leakage and "edge effect" caused by VTs, which improve the overall MSE performance significantly. Both numerical and simulation results demonstrate that the proposed method gives a better performance than conventional DFT-based channel estimations and achieves high robustness to VTs. Furthermore, no extra computational complexity arises from our approach. In summary, the proposed ECDFT-PR channel estimation is a cost-effective scheme which is particularly suitable for hardware realization.

## Acknowledgment

This work was supported in part by the National 863 High Technology Research and Development Program of China under Grant NO. 2009AA011502, and by the National Natural Science Foundation of China under Grant NO. 60772113.

## References

[1] J. Cimini, L., "Analysis and simulation of a digital mobile channel using orthogonal frequency division multiplexing," *IEEE Trans. Commun.*, vol. 33, no. 7, pp. 665–675, Jul 1985.

[2] IEEE 802.16 Task Group m (TGm), "IEEE 802.16m System Description Document (SDD)," Sep. 2009. [Online]. Available: http://www.ieee802.org/16/tgm/docs/80216m-09/0034r2.zip

[3] 3GPP TR 36.814 V1.5.0, "Further Advancements for E-UTRA Physical Layer Aspects," Nov. 2009. [Online]. Available: http://www.3gpp.org/ftp/Specs/archive/36 series/36.211

[4] G. L. Stuber, J. R. Barry, S. W. McLaughlin, Y. Li, M. A. Ingram, and T. G. Pratt, "Broadband MIMO-OFDM wireless communications," *Proc. IEEE*, vol. 92, no. 2, pp. 271–294, Feb 2004.

[5] J. Hui-ying, A. Jian-ping, B. Xiang-yuan, and W. Hua, "A novel method of channel estimation in broadband MIMO-OFDM systems," in *Proc. IEEE Wireless Communications and Networking Conference WCNC 2007*, 11–15 March 2007, pp. 836–840.

[6] J. Haifang and S. Yin, "An efficient iterative DFT-based channel estimation for MIMO-OFDM systems on multipath channels," in *Proc. Third International Conference on Communications and Networking in China ChinaCom 2008*, 25–27 Aug. 2008, pp. 45–49.

[7] H. O. A. Higashinaka, M.; Kubo, "Channel estimation with interference cancellation for a MIMO receiver using iterative equalization and decoding," *Personal, Indoor and Mobile Radio Communications, 2008. PIMRC 2008. IEEE 19th International Symposium on Digital Object Identifier*, pp. 1–5, 2008.

[8] M. Ghogho, "On optimum pilot design for OFDM systems with virtual carriers," in *Proc. IEEE EURASIP Int. Symp on Communications, Control and Signal Processing*, 2006.

[9] S. Adireddy, L. Tong, and H. Viswanathan, "Optimal placement of training for frequency-selective block-fading channels," *IEEE Trans. Inf. Theory*, vol. 48, no. 8, pp. 2338–2353, Aug. 2002.

[10] O. Edfors, M. Sandell, J. J. van de Beek, S. K. Wilson, and P. O. Borjesson, "Analysis of DFT-based channel estimators for OFDM," *Wireless Personal Commun*, vol. 12, no. 1, pp. 55–70, Jan 2000.

[11] ITU-R WP5D, "Guidelines for evaluation of radio interface technologies for IMT-Advanced." 2008. [Online]. Available: http://www.itu.int/publ/R-REP-M.2135-2008/en